

Low-Ceiling-Temperature Polymer Microcapsules with Hydrophobic Payloads via Rapid Emulsion-Solvent Evaporation

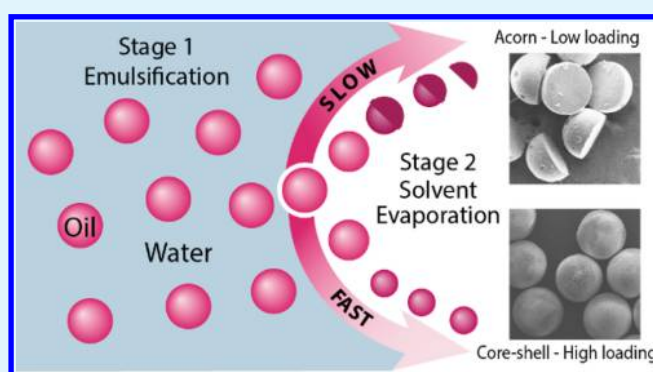
Shijia Tang,^{†,‡,§} Mostafa Yourdkhani,^{†,‡} Catherine M. Possanza Casey,^{‡,||} Nancy R. Sottos,^{‡,§} Scott R. White,^{*,‡,⊥} and Jeffrey S. Moore^{*,‡,§,||} 

[†]Beckman Institute for Advanced Science and Technology, [§]Department of Materials Science and Engineering, [⊥]Department of Aerospace Engineering, and ^{||}Department of Chemistry, University of Illinois at Urbana–Champaign, Urbana, Illinois 61801, United States

Supporting Information

ABSTRACT: We report a microencapsulation procedure based on rapid solvent evaporation to prepare microcapsules with hydrophobic core materials and low-ceiling-temperature polymer shell wall of cyclic poly(phthalaldehyde) (cPPA). We use and compare microfluidic and bulk emulsions. In both methods, rapid solvent evaporation following emulsification resulted in kinetically trapped core–shell microcapsules, whereas slow evaporation resulted in acorn morphology. Through the systematic variation of encapsulation parameters, we found that polymer-to-core weight ratios higher than 1 and polymer concentrations higher than 4.5 wt % in the oil phase were required to obtain a core–shell structure. This microencapsulation procedure enabled the fabrication of microcapsules with high core loading, controlled size, morphology, and stability. This procedure is versatile, allowing for the encapsulation of other hydrophobic core materials, i.e., mineral oil and organotin catalyst, or using an alternative low-ceiling-temperature polymer shell wall, poly(vinyl *tert*-butyl carbonate sulfone).

KEYWORDS: low-ceiling-temperature polymers, solvent evaporation, hydrophobic payloads, microfluidic emulsification, bulk emulsification



INTRODUCTION

Microcapsule-based self-healing composite materials have been used to restore mechanical, optical, and electrical properties to damaged materials.^{1–7} Mechanical damage triggers the release of microcapsule payloads into the damage zone, initiating the healing process. However, the release of payloads on-demand via nonmechanical triggering events remains an active area of development in self-healing materials.^{8–10} For example, pH and redox responsive microcapsules enable the development of self-protective coatings by delivering anticorrosive agents in response to local pH variation or electrochemical reaction.^{11–13} Alternatively, thermoresponsive microcapsules incorporated in Li-batteries achieve autonomic shutdown at elevated temperature.¹⁴ A promising approach for developing stimuli-responsive microcapsules is to employ a kinetically stabilized, low-ceiling-temperature polymer as the shell wall. This class of polymers undergoes cascade depolymerization when end-capping groups are removed and/or the polymer backbones are cleaved by environmental triggers. The polymers rapidly lose mechanical integrity once triggered and provide a convenient means for the on-demand delivery of payloads. Choices for the low-ceiling-temperature polymers are plentiful and include polycarbonates,^{15–18} polyaldehydes,^{19–21} and poly(olefin sulfone)s.^{22–25} However, using these low-ceiling-

temperature polymers as the microcapsule shell wall is often challenging, because of strict requirements on the compatibility of the shell wall and payload materials, while maintaining shell wall stability under encapsulation conditions.

In previous studies, fabrication of microcapsules using low-ceiling-temperature polymers has relied on a water-in-oil-in-water (W/O/W) double emulsion template generated using a flow-focusing microfluidic device. Fluoride-responsive microcapsules with silyl ether-capped linear poly(phthalaldehyde) (PPA) as the shell wall were fabricated using this approach.²⁶ Acid-triggered microcapsules have also been demonstrated using poly(o-(α -methyl)vinylbenzaldehyde) as the shell wall.²⁷ Beyond these few examples, an alternative, scalable method for the encapsulation of hydrophobic payloads in low-ceiling-temperature polymers is an important target for on-demand, environmentally triggered microcapsule release.

Solvent evaporation is a promising route to fabricate polymer microcapsules with hydrophobic payloads for controlled release.^{28–38} Typically, an oil-in-water (O/W) single emulsion template is generated by agitation, followed by solvent

Received: April 14, 2017

Accepted: May 25, 2017

Published: May 25, 2017



evaporation to form microcapsules. The oil phase is a ternary system, containing a polymer, a volatile solvent (*vs*) and a nonvolatile nonsolvent (*nvns*). The polymer is soluble in the *vs* and immiscible with the *nvns*. Before emulsification, the mixing ratios of the three components are adjusted to form a homogeneous solution. After emulsification, the *vs* is removed by evaporation, leaving the polymer as the shell wall and the *nvns* as the payload. As predicted by canonical spreading coefficient theory³⁹ a core-shell microcapsule morphology is thermodynamically favored only when the interfacial tensions (γ) between polymer (p), core (o), and surfactant (w) satisfy relations 1–3

$$\gamma_{wp} - (\gamma_{ow} + \gamma_{op}) < 0 \quad (1)$$

$$\gamma_{op} - (\gamma_{wo} + \gamma_{wp}) < 0 \quad (2)$$

$$\gamma_{ow} - (\gamma_{po} + \gamma_{pw}) > 0 \quad (3)$$

As such, the combinations of polymer, core, and surfactant are limited and the solvent evaporation method has mostly been applied in the formation of microcapsules from poly(methyl methacrylate),^{40,31} polystyrene,²⁸ poly(lactide),³² and cellulose.⁴¹ Here, we report a microencapsulation procedure using rapid solvent evaporation to prepare microcapsules with hydrophobic core materials and a low-ceiling-temperature polymer shell wall, cyclic poly(phthalaldehyde) (cPPA).²⁰ We demonstrated the ability to fabricate a core-shell microcapsule via kinetic trapping mechanism as a result of rapid solvent removal, whereas an acorn-shaped microcapsule morphology was obtained under slow solvent evaporation (Figure 1). By

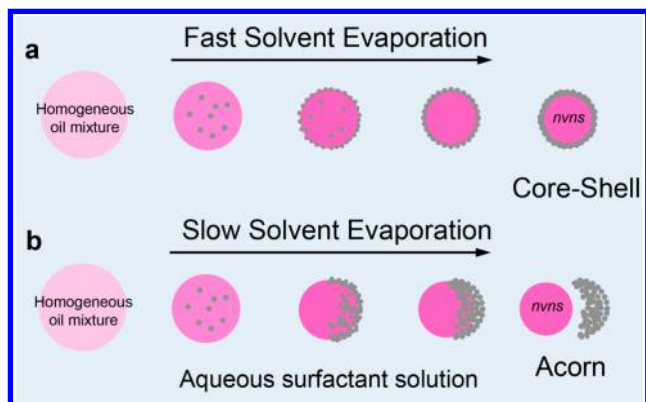


Figure 1. Schematic illustration of the effect of solvent evaporation rate on microcapsule formation. Pink circles represent the oil-in-water droplets; gray dots represent cPPA polymer precipitated in the oil droplet. (a) Core-shell microcapsules were formed under rapid solvent evaporation as cPPA migrated to the O/W interface. (b) Acorn-shaped morphologies were formed under slow evaporation as cPPA migrated to one side of the O/W droplet, leaving the polymer shell wall partially enclosing the core (payload). After rinsing the microcapsules, the payload and polymer were separated, resulting in hemispherical polymer morphologies.

tuning the polymer-to-core weight ratios and polymer concentrations in the oil phase, we identified the boundary conditions to kinetically trap the core-shell structure. This method was used to encapsulate a variety of hydrophobic payloads including a corrosion inhibitor jojoba oil (JJB), mineral oil (MO), and the organotin catalyst dibutyltin dilaurate (DBTL). We also examined another low-ceiling-

temperature polymer, poly(vinyl *tert*-butyl carbonate sulfone) (PVtBCS),²² as an alternative shell wall material for the fabrication of stimuli-responsive microcapsules.

EXPERIMENTAL SECTION

Materials and Instruments. Unless otherwise noted, all starting materials were obtained from Sigma-Aldrich and used as received. The monomer *o*-phthalaldehyde (*o*-PA, 98%, Alfa-Aesar) was purified by hot filtration followed by a single recrystallization according to a literature procedure.²⁰ *tert*-Butyl hydroperoxide (*t*-BuOOH) was purchased from Sigma-Aldrich as a 5–6 M solution in decane and was assumed to be 5.5 M for all calculations. Sulfur dioxide (anhydrous, 99.98%) was purchased from Airgas in lecture bottles. Dichloromethane was obtained from an anhydrous solvent delivery system equipped with activated alumina columns. All glassware was oven-dried prior to use. The synthesis of cyclic poly(phthalaldehyde) (cPPA) and synthesis of the poly(olefin sulfone)s followed previous literature procedures with minor modifications.^{20,22} The polymer structure was confirmed on ¹H NMR spectra using a Varian 500 MHz spectrometer.

Analytical gel permeation chromatograph (GPC) analyses were performed with a Waters1515 isocratic HPLC pump, a Waters (2998) photodiode array detector, a Waters (2414) refractive index detector, a Waters (2707) 96-well autosampler, and a series of 4 Waters HR Styragel columns (7.8 × 300 mm, HR1, HR3, HR4, and HR5) in THF at 30 °C. The GPC was calibrated using monodisperse polystyrene standards.

The thermal properties of microcapsules were characterized on a TA Instrument Q50 thermogravimetric analysis (TGA) and a Mettler Toledo TGA851^o. Dynamic TGA experiments were performed by heating samples from 25 to 650 °C at a rate of 10 °C/min. A purge gas of N₂ at 60 mL/min was used for all experiments.

The loading efficiency is calculated by comparing the actual JJB core loading (L_{JJB}) in microcapsules with the theoretical JJB core loading ($L_{\text{JJB}}^{\text{th}}$) in the microcapsules.

$$\text{loading efficiency}(\xi) = \frac{L_{\text{JJB}}}{L_{\text{JJB}}^{\text{th}}} 100\% \quad (4)$$

The L_{JJB} was determined by the remained wt % from TGA profiles at 250 °C. And the theoretical $L_{\text{JJB}}^{\text{th}}$ is calculated from

$$L_{\text{JJB}}^{\text{th}} = \frac{m_{\text{JJB}}}{m_{\text{JJB}} + m_{\text{cPPA}}} 100\% \quad (5)$$

where m_{JJB} and m_{cPPA} are the initial mass of JJB and cPPA used for microcapsules preparation.

The distribution coefficient of Nile red in the shell wall cPPA and the core materials JJB oil is determined by a fluorospectrometer (HORIBA Scientific, FluoroMax-4). To quantify the Nile red concentration, the mass of microcapsules samples (bulk emulsification, $m_{\text{cPPA}}/m_{\text{JJB}}/m_{\text{DCM}} = 1/1/13.26$) were accurately measured. The microcapsules were crushed between two glass slides, rinsed repeatedly with heptane to dissolve the released core materials from the mechanically crushed microcapsules. The broken shell wall was then centrifuged, collected, and dried before dissolving in DCM. Fluorescence intensities of the core Nile red/heptane solution and shell wall Nile red/DCM solution were measured by the fluorospectrometer. The concentration of Nile red in the core or shell wall was determined from the Nile red calibration curve (Figure S1) in the corresponding solvent. The distribution coefficient (m/m) of Nile red in JJB/cPPA was calculated as 0.557 ± 0.050 based on three parallel experiments.

Visualization of microcapsule morphology and triggering experiments was performed on a Leica DMR optical microscope (fluorescence mode). Scanning electron microscopy (SEM) was performed using a Hitachi S-4700. Before SEM imaging, samples were sputter-coated with Au/Pd to eliminate surface charging effects. ImageJ software was used to measure the diameter of microcapsules.

The density of polymer was measured by gas pycnometer (Quantachrome Instrument Ultrapyc 1200e) using pulse mode.

Ternary Phase Diagram. The ternary phase diagram for cPPA, dichloromethane (DCM, *vs*) and JJB (*nvns*) was determined by mixing accurate amounts of the three components in a 7 mL glass vial.^{28,34} The total mass of the mixed solution with the glass vial and stir bar was recorded. Then, the solvent was evaporated while stirring at 25 °C until the solution became cloudy. The total mass was reweighed immediately and mass difference was attributed to the evaporation of DCM only. Weight fractions of cPPA, JJB, and DCM at the phase boundary were then determined. Fourteen samples were prepared with different mass compositions to complete the phase boundary diagram.

Microcapsule Fabrication by Microfluidic Emulsification. cPPA microcapsules were fabricated using a flow-focusing microfluidic device to prepare emulsions, followed by solvent evaporation. This technique enables controlled formation of emulsion droplets with approximately identical geometry,^{42,43} which is quite useful for thorough characterization of microcapsules properties. Microfluidic devices were composed of two tapered cylindrical glass capillaries inserted into the opposing ends of a square glass capillary (Figure S2). A homogeneous mixture of various compositions of cPPA, JJB, and DCM was injected into the left cylindrical capillary. Nile red was added in the oil phase to facilitate visualization. A 2.5 wt % aqueous solution of the emulsifier poly(vinyl alcohol) (PVA, $M_w = 89\,000$ – $98\,000$, 99% hydrolyzed) was injected into the region between the right capillary and square capillary. O/W droplets formed as the two flows merged at the orifice of the collection tube. The generated droplets were collected in a round-bottom flask filled with 1 wt % PVA solution. Immediately after collection, flasks were connected to a rotary evaporator to remove DCM at reduced pressure for 1 h (rapid evaporation). For slower evaporation, the emulsion was stirred (<30 rpm) at ambient conditions until evaporation was complete (ca. 24 h).

To monitor DCM evaporation, aliquots of the emulsion were taken at periodic time intervals and imaged by fluorescence microscopy (FM) to observe variations in capsules morphology and diameter. A total of 15–20 droplets were imaged at each time point. Assuming the volume loss in the droplets was only due to DCM evaporation, and knowing the initial weight percentage and density of DCM, JJB, and cPPA, we calculated the residual DCM based on the reduction in microcapsules diameter (Figure S3).

After evaporation, microcapsules were collected by vacuum filtration and washed with 500 mL deionized water to remove residual surfactant followed by another wash with 50 mL of heptane to remove residual organics. Microcapsules were subsequently dried at room temperature for 24 h to complete the drying process.

Microcapsule Fabrication by Bulk Emulsification. cPPA microcapsules were fabricated by bulk emulsification followed by solvent evaporation. A homogeneous mixture of various compositions of cPPA, JJB, and DCM was prepared. The mixture was added dropwise into a 1 wt % PVA solution under 400 rpm agitation. The container was capped and the O/W emulsion was stirred for another 10 min. The emulsion was then poured into 100 mL of 1 wt % PVA solution in a round-bottom flask, and the solvent DCM was removed by rotary evaporation for 1 h at reduced pressure or following slow evaporation procedure as used in microfluidic method. The resulting microcapsules were cleaned and dried by the same procedure used in microfluidic method.

Release Profile Measurement. The release profiles of microcapsules were obtained based on the change of Nile red fluorescence intensity inside the microcapsules, following a previous literature procedure with minor modifications.²⁷ A sample of 10–20 microcapsules was placed in a 96-well plate. Heptane, a nonsolvent for the shell wall polymer cPPA, was used as a medium to prepare trifluoroacetic acid (TFA) solutions. It should be noted that heptane may have a plasticizing effect on cPPA polymers. The TFA-heptane solution was added to samples of cPPA microcapsules. The well plate was then sealed to prevent solution evaporation. Fluorescence microscopy images were captured at designated time intervals over a period of 48 h. For each sample, all imaging parameters, such as exposure time, color contrast, and color balance were held constant

during data collection. To determine the release profile, ImageJ was used to measure the mean gray value of the microcapsules. The change of mean gray value represents the remaining core percentage by normalization. For each concentration, at least three samples were prepared and imaged.

RESULTS AND DISCUSSION

Microcapsule Fabrication via Rapid Solvent Evaporation. Core–shell microcapsules were successfully prepared through the generation of an O/W emulsion followed by rapid solvent evaporation. Two low-ceiling-temperature polymers, cPPA and PVtBCS were used as the shell wall materials, separately. cPPA was synthesized by cationic polymerization using $\text{BF}_3 \cdot \text{OEt}_2$ as an initiator ($M_n = 55$ kDa, PDI = 1.6, Table S1).²⁰ PVtBCS was synthesized by free radical polymerization using tBuOOH as an initiator ($M_n = 19$ kDa, PDI = 3.2, Table S2).²² Both microfluidic and bulk emulsification methods were employed to substantiate our hypothesis of the effect of solvent evaporation rate on microcapsule morphology. For most studies, we used cPPA as the shell wall polymer, JJB as core materials (*nvns*) and DCM as *vs* ($m_{\text{cPPA}}/m_{\text{JJB}}/m_{\text{DCM}} = 1/1/13.26$). An oil-soluble fluorescence dye, Nile red, was added to the organic phase to assist visualization.

Before emulsification, a homogeneous oil mixture of cPPA, JJB, and DCM was prepared with the guidance of a ternary phase diagram at 25 °C (Figure 2). The phase boundary

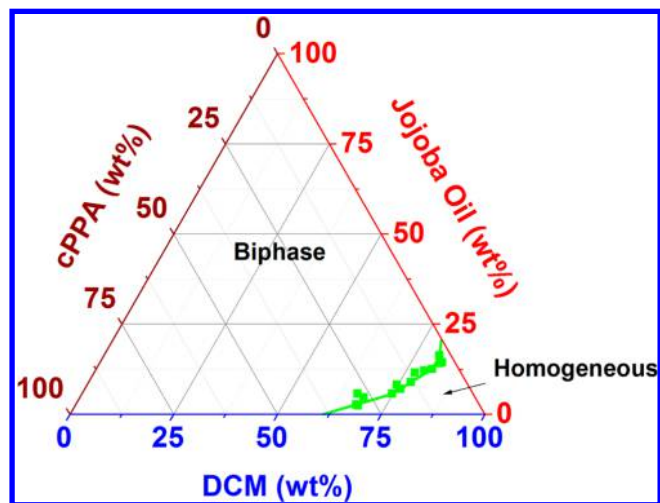


Figure 2. cPPA-JJB-DCM ternary phase diagram at 25 °C. The green squares denote cloud points for different compositions of cPPA, JJB, and DCM. Green line was drawn to guide the visualization. Below the green line is the homogeneous regime; above the green line is the biphasic regime.

(green) demarcates solutions that are homogeneous (below) and biphasic (above). Before emulsification, the mass ratio of $m_{\text{cPPA}}/m_{\text{JJB}}/m_{\text{DCM}}$ in the oil mixture must be in the homogeneous regime to achieve a core–shell structure. Immediately after emulsification, DCM was removed rapidly under reduced pressure or slowly under ambient pressure in order to form the microcapsule shell wall.

In our study, we found that the core–shell structure was favored when DCM was removed rapidly. To illustrate the effect of solvent evaporation rate, we monitored microcapsule morphology by microscopy during solvent evaporation (Figure 3). Immediately after microfluidic emulsification, monodisperse droplets were obtained (Figure 3a). After evaporation under

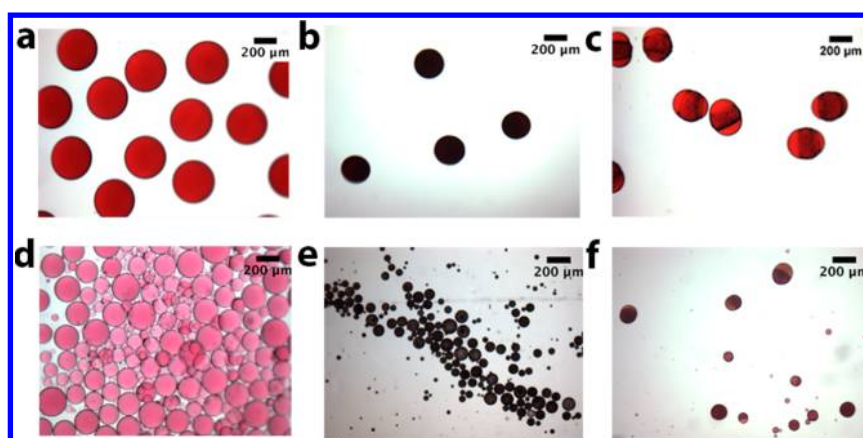


Figure 3. Optical microscopy images of O/W droplets during solvent evaporation. O/W droplets collected immediately after (a) microfluidic emulsification and (d) bulk emulsification. Sphere-shaped intermediates after 30 min evaporation at reduced pressure (fast evaporation) obtained from (b) microfluidic emulsification and (e) bulk emulsification. Acorn-shaped morphologies after 30 min evaporation at ambient pressure (slow evaporation) obtained from (c) microfluidic emulsification and (f) bulk emulsification.

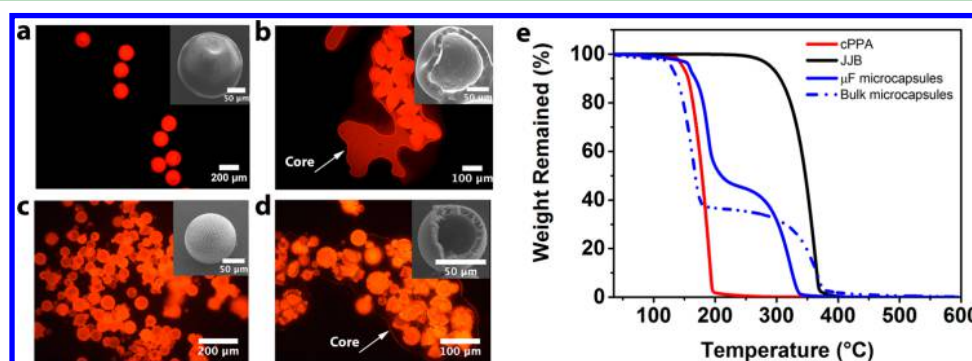


Figure 4. Core-shell microcapsules characterization. Microcapsules fabricated from microfluidic emulsification (a) before crushing and (b) after crushing, showing the release of core material JJB (arrow); insets are intact and ruptured microcapsules showing exterior and shell wall morphologies. Microcapsules fabricated from bulk emulsification (c) before crushing and (d) after crushing, showing the release of core material JJB (arrow); insets are intact and ruptured microcapsules showing exterior and shell wall morphologies. (e) Thermal analysis of microcapsules fabricated with microfluidic emulsification (solid blue) and bulk emulsification (dashed blue). Thermal analysis of cPPA (red) and JJB (black) were plotted to assist the quantification of individual component loading in the microcapsules.

reduced pressure for 30 min, sphere-shaped intermediates were observed (Figure 3b). The diameter was reduced in the transition from the droplets ($416.3 \pm 3.0 \mu\text{m}$) to the microcapsules ($268.0 \pm 4.7 \mu\text{m}$), indicating the loss of DCM (Figure S3). After another 30 min evaporation, the final products were filtrated, cleaned and dried. SEM images revealed that the products were monodispersed, sphere-shaped, core-shell microcapsules (Table S3, Figure S4a–e). In contrast, when the emulsion was allowed to evaporate under ambient pressure for 30 min, acorn-shaped morphologies were observed (Figure 3c). The final products were found to possess a hemispherical structure (Figure S4f). The O/W droplet morphology evolution under slow solvent evaporation is illustrated schematically in Figure 1b. Partially enclosed structures developed as the polymer phase migrated to one side of the droplet. Filtering and rinsing the acorn-shaped structures resulted in the removal of the JJB core and the formation of hemispherical polymer particles (Figure S4f).

To validate the critical role of solvent evaporation rate on the formation of core-shell microcapsules, we performed parallel experiments with bulk emulsification. The O/W emulsion was generated by mechanical agitation (Figure 3d), followed by rapid or slow solvent evaporation. Similar to the microfluidic results, under rapid evaporation, a spherical structure was

formed and a core-shell morphology was obtained (Figure 3e, Table S4, Figure S5a–c, e, f). When the evaporation rate was reduced, acorn-shaped morphologies were observed and final products were hemispherical (Figure 3f, Figure S5k).

Using rapid solvent evaporation to obtain core-shell structure microcapsules is contradictory to previous studies by Dowding et al. where slow solvent evaporation yielded better shell wall structures.²⁸ Their observations are explained by the canonical spreading coefficient theory developed by Torza and Mason.³⁹ This theory suggests that obtaining a core-shell structure after the *vs* evaporates requires the interfacial tension (γ) of any two phases in polymer (p), core (o), and surfactant (w) to satisfy the above-mentioned relations 1–3. Under these relations, the core-shell structure is in a thermodynamic equilibrium state and a slower solvent evaporation rate allows enough time for polymers to uniformly migrate onto the O/W interface,^{35,36} minimizing kinetic factors and forming a spherical core-shell structure with better barrier properties as shown by Dowding et al. In the present work, however, the acorn-shaped morphologies obtained under slow evaporation indicated that the spreading of p phase over o phase resulted in partial enclosure due to the thermodynamic driving forces; apparently the core-shell structure is a nonequilibrium state. By increasing the evaporation rate, the

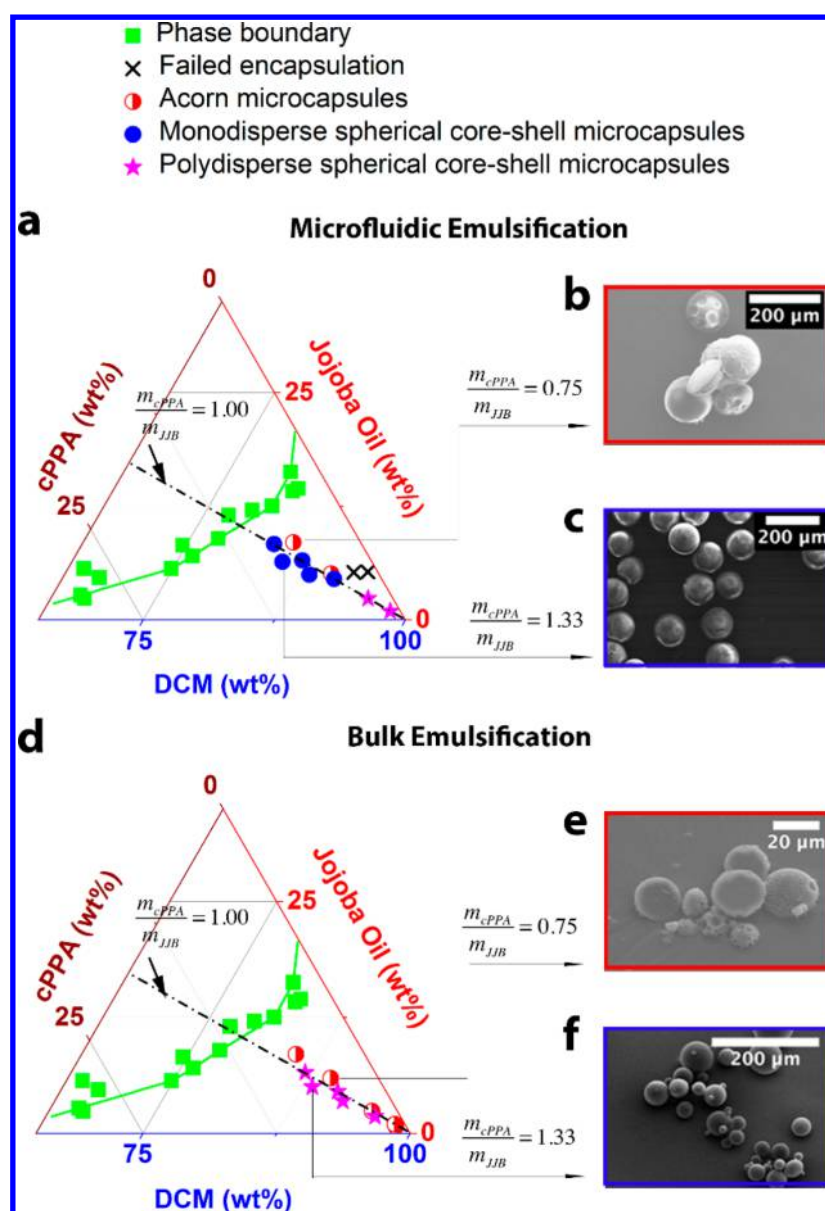


Figure 5. Effect of composition ratios on cPPA encapsulation. The cPPA-JJB-DCM phase boundary (green squares) is replotted from Figure 2. The results of encapsulations over a range of chemical compositions are denoted on the ternary phase diagram for (a–c) microfluidic emulsification and (d–f) bulk emulsification. (b, e) are SEM images for $m_{cPPA}/m_{JJB} = 0.75$. (c, f) SEM images for $m_{cPPA}/m_{JJB} = 1.33$. Note: the black dashed line is the midline of the phase diagram triangle, and the composition located on the midline has m_{cPPA}/m_{JJB} value of 1.00.

core–shell structure is kinetically trapped, overcoming the thermodynamic tendency to form acorn-shaped morphologies.^{35,36}

Microcapsule Diameter and Shell Wall Thickness.

Using the microfluidics approach, we were able to precisely tune the microcapsule diameter (D) from $149.3 \pm 7.5 \mu\text{m}$ to $244.1 \pm 5.7 \mu\text{m}$ by adjusting the flow ratio of the water and oil phases (Q_w/Q_o) from 120 to 10 (Figure S6), while maintaining $m_{cPPA}/m_{JJB}/m_{DCM} = 1/1/13.26$. A linear relationship was found between the logarithm values of D and Q_w/Q_o .

The shell wall thickness was measured by imaging manually ruptured cPPA microcapsules. SEM images revealed that the shell wall thickness varied from $12.4 \pm 1.9 \mu\text{m}$ to $18.7 \pm 4.1 \mu\text{m}$ (Figure S7). The shell wall thickness was approximately 10% of the microcapsule diameter (Table S5, column 4). The ability to independently control the shell wall thickness of microcapsules has not been the focus of this study. However, the shell wall

thickness depends on m_{cPPA}/m_{JJB} and the diameters of generated oil droplets

In bulk emulsification, microcapsules showed a polydisperse size distribution (Figure S8). When the agitation rate was maintained at 400 rpm and the oil phase composition was $m_{cPPA}/m_{JJB}/m_{DCM} = 1/1/13.26$, the diameter ranged from 10 to 120 μm . Representative shell wall images are shown in Figure S9. Because of the polydispersity of microcapsules, the ratio of the shell wall thickness to the microcapsule diameter could not be estimated.

Core Materials Loading. Successful loading of the target payload (JJB) was qualitatively examined by fluorescence microscopy (FM) after compressing few microcapsules between two glass slides. As shown in Figure 4b, d, fluorescent liquid (Nile red in JJB) was released upon the rupture of microcapsules. Thermogravimetric analysis (TGA) was performed to quantify the loading of JJB in microcapsules (Figure

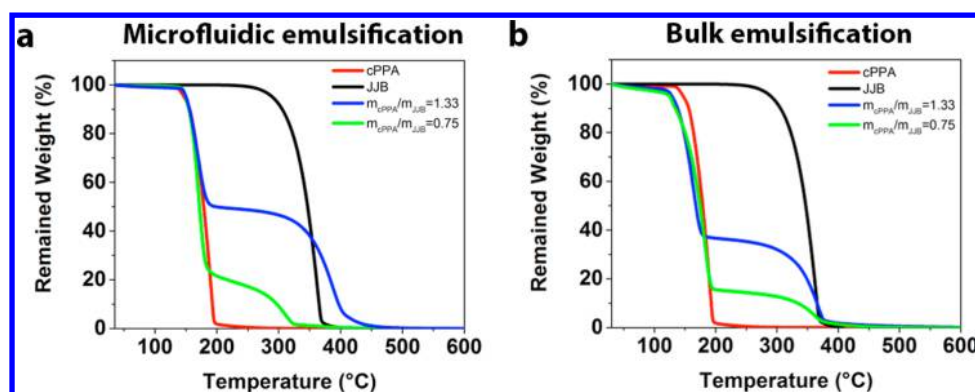


Figure 6. Thermal analysis of microcapsules fabricated by (a) microfluidic emulsification and (b) bulk emulsification. Capsules made with $m_{\text{cPPA}}/m_{\text{JJB}} = 1.33$ (blue) and $m_{\text{cPPA}}/m_{\text{JJB}} = 0.75$ (green) are plotted together with neat cPPA (red) and JJB (black).

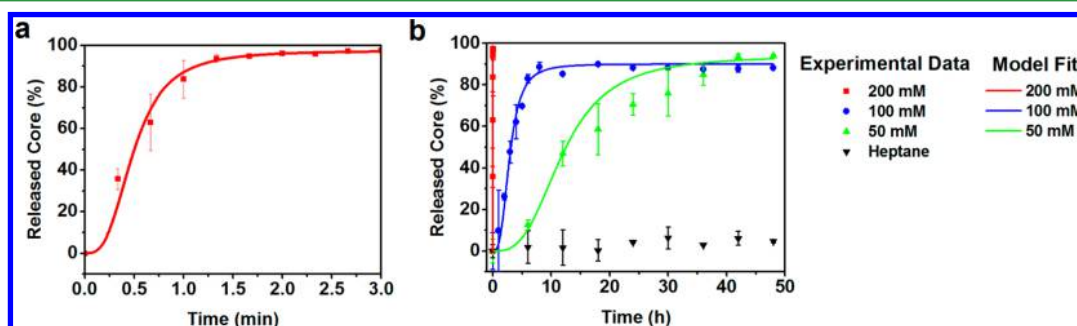


Figure 7. Microcapsules release profiles. (a) Release profile in response to 200 mM TFA in heptane. (b) Release profiles in response to various acid concentrations and pure heptane.

4e). Thermal profiles of cPPA microcapsules exhibited distinct mass loss at ca. 150 °C and at ca. 300 °C, attributed to the thermal decomposition of cPPA and evaporation of core JJB oil, respectively. Microcapsules fabricated using microfluidics contained approximately 44.7 wt % JJB (blue, solid line, $\xi = 89.4\%$) and microcapsules from bulk emulsification contained 36.8 wt % JJB (blue, dashed line, $\xi = 73.6\%$). In contrast, the thermal profiles of the acorn-shaped microcapsules obtained from the slow solvent evaporation revealed that less than 20 wt % JJB was encapsulated in both microfluidic (Figure S10, entry M12, $\xi = 12.4\%$) and bulk emulsification methods (Figure S11, entry B11, $\xi = 27.2\%$).

Effect of Component Materials Concentrations on Microcapsule Morphology and Loading. On the basis of the observations described above, we hypothesized the existence of a boundary condition for cPPA-JJB-DCM compositions at which the kinetic trapping effect overcomes thermodynamic driving forces. To determine the criteria for obtaining core-shell microcapsules under rapid solvent evaporation, we tested cPPA-JJB-DCM ternary system with varied compositions and examined the encapsulation products by SEM and FM. We summarized microcapsule morphology with respect to the corresponding cPPA-JJB-DCM compositions in the ternary phase diagram shown in Figure 5.

The effect of polymer-to-core mass ratios ($m_{\text{cPPA}}/m_{\text{JJB}}$) was investigated for a range of values from 1.33 to 0.17 (Table S3, Figure S4). When $1.00 \leq m_{\text{cPPA}}/m_{\text{JJB}} \leq 1.33$, the encapsulation produced spherical core-shell microcapsules (Table S3, entries M1–M7). When the $m_{\text{cPPA}}/m_{\text{JJB}}$ was 0.88 and 0.75, acorn-shaped microcapsules were obtained (Table S3, entry M8, M11). Further reduction of the $m_{\text{cPPA}}/m_{\text{JJB}}$ ratio to 0.44 and 0.17, yielded no microcapsules after evaporation (Table S3,

entry M9, M10). Representative SEM images are shown for acorn and core-shell microcapsules (Figure 5b, c). These results indicate that $m_{\text{cPPA}}/m_{\text{JJB}} \geq 1$ is required for obtaining the core-shell structure.

We also investigated the effect of polymer weight concentration in the oil phase ($m_{\text{cPPA}}/m_{\text{oil phase}}$) on micro-encapsulation. The $m_{\text{cPPA}}/m_{\text{oil phase}}$ ratio was adjusted from 0.010 to 0.084, while maintaining the $m_{\text{cPPA}}/m_{\text{JJB}}$ value at 1.00 (Table S3, entries M3–M7, Figure S4). When $0.045 \leq m_{\text{cPPA}}/m_{\text{oil phase}} \leq 0.084$, monodisperse spherical microcapsules were produced (Table S3, entries M3–M5). When $m_{\text{cPPA}}/m_{\text{oil phase}}$ was lowered to 0.024 and 0.010 (Table S3, entries M6–M7), the encapsulation products were polydisperse spherical microcapsules. SEM images also revealed that when $m_{\text{cPPA}}/m_{\text{oil phase}}$ was lower than 0.024, the shell walls exhibited microcracks (Figure S4f, g). Therefore, $m_{\text{cPPA}}/m_{\text{oil phase}} \geq 0.045$ is another requirement to obtain a core-shell structure.

To confirm these requirements, we performed bulk emulsification experiments with varied cPPA-JJB-DCM compositions (Table S4, Figure S5). In good agreement with the microfluidic experiments, the composition requirements for kinetically trapping the core-shell structure were $m_{\text{cPPA}}/m_{\text{JJB}} \geq 1$ and $m_{\text{cPPA}}/m_{\text{oil phase}} \geq 0.045$ (Figure Sd–f, Table S4, Figure S5).

The loading of JJB in microcapsules with varied $m_{\text{cPPA}}/m_{\text{JJB}}/m_{\text{DCM}}$ was examined by TGA (Figure 6). At $m_{\text{cPPA}}/m_{\text{JJB}} = 1.33$, approximately 48.7 and 35.3 wt % JJB oil loading was obtained by microfluidic and bulk emulsification methods, respectively. At $m_{\text{cPPA}}/m_{\text{JJB}} = 0.75$, approximately 17.2 and 14.4 wt % JJB oil loading was obtained by microfluidic and bulk emulsification methods, respectively. Generally, a core-shell morphology led to higher payload (JJB) content than acorn-shaped structures.

Triggered Release from Microcapsules. cPPA is known as an acid-responsive polymer.^{44,45} We evaluated the release profiles of cPPA microcapsules under acidic conditions (Figure S12). Because the release kinetics can vary with the dimension of capsules and shell wall thickness, we only tested microcapsules fabricated by microfluidic emulsification with composition of $m_{\text{cPPA}}/m_{\text{JJB}}/m_{\text{DCM}} = 1/1/13.26$, which has moderate size and shell wall thickness (Table S3, entry M4). For release analysis, we selected heptane as the suspension medium. Heptane is a nonsolvent for cPPA and its hydrophobicity will not inhibit JJB oil release. The release of the JJB oil core was measured by monitoring the fluorescent intensity of the microcapsules as a function of time. The release of encapsulated JJB oil in pure heptane at different concentrations of TFA is plotted in Figure 7. In pure heptane, less than 5% release of JJB was observed after 48 h, indicating the microcapsules are stable under neutral conditions. As the concentration of acid in heptane increased, the core material (JJB) was released at a faster rate, indicating more rapid depolymerization of the cPPA shell wall. The core release from cPPA microcapsules is modeled by fitting the results to an empirical logistic dose response equation⁴⁶

$$R = \frac{R_0 - R_f}{1 + (t/t_{1/2})^n} + R_f \quad (6)$$

where R_0 is the initial release value, R_f is the final release value, $t_{1/2}$ is the half-life and n is the order exponent. Fitting parameters are summarized in Table 1. The exponent n of this logistic fit is found to be ca. 3. A smaller half-life value indicates a faster payload release rate.

Table 1. Release Profile Model Parameters

concentration (mM)	R_0	R_f	n	$t_{1/2}$ (h)
50	0	93.9	3	12.0
100	0	90.0	3	2.9
200	0	97.4	3	0.008

Encapsulation of Other Core Materials. To illustrate the generality of our approach, we encapsulated other hydrophobic core materials using microfluidic emulsification and rapid solvent evaporation. Following one of the compositions satisfying the kinetic trapping conditions, $m_{\text{cPPA}}/m_{\text{JJB}}/m_{\text{DCM}} = 1/1/13.26$, we replaced JJB with mineral oil (MO) or a liquid tin catalyst dibutyltin dilaurate (DBTL). The spherical, core-shell structure was confirmed by SEM images as shown in Figure S13. However, for these hydrophobic payloads, the loading efficiency is hard to estimate because of the lack of distinct two-stage weight loss as observed in cPPA/JJB microcapsules.

To further test the generality of the approach, we also successfully encapsulated JJB in a poly(olefin sulfone) shell wall. We selected PVtBCS as an alternative shell wall material because of its responsiveness to thermal stimuli (decomposition onset temperature is 91 °C).²² Using the condition, $m_{\text{PVtBCS}}/m_{\text{JJB}}/m_{\text{CHCl}_3} = 1/0.75/14.92$, we obtained polydisperse core-shell microcapsules with PVtBCS shell wall via microfluidic emulsification and rapid solvent evaporation (Figure S13) with core materials loading about ~51.5 wt %. By comparing to the feed ratio of core materials, we estimated the loading efficiency to be ~120%. We attributed this number to the loss of shell

wall materials PVtBCS during the encapsulation procedure, because of its slow degradation in ambient environment.²²

CONCLUSIONS

We demonstrated a facile and robust methodology to encapsulate hydrophobic payloads in the low-ceiling-temperature polymer, cPPA. Experimental data suggests that core-shell microcapsules, obtained by rapid solvent removal, are the kinetically favored structure. Microcapsule morphology and core loading were controlled by varying the chemical composition and polymer concentrations in the oil phase. By adjusting the ratio of water and oil flow rates, we obtained monodisperse microcapsules with controllable size. The microcapsules exhibited stability in neutral conditions and fast release under acidic conditions. This encapsulation technique is a powerful tool that is applicable to various core materials and potentially other low-ceiling-temperature polymers. Additionally, this method is relevant to both microfluidic and bulk emulsification, opening opportunities for the scalable production of stimuli-responsive microcapsules for self-protective coating applications.

ASSOCIATED CONTENT

Supporting Information

The Supporting Information is available free of charge on the ACS Publications website at DOI: 10.1021/acsami.7b05266.

Experimental procedures, synthesis, encapsulation parameters, TGA, SEM, FM, triggering experiments (PDF)

AUTHOR INFORMATION

Corresponding Authors

*E-mail: jmoore@illinois.edu.

*E-mail: swhite@illinois.edu.

ORCID

Jeffrey S. Moore: 0000-0001-5841-6269

Author Contributions

[†]S.T. and M.Y. contributed equally. The manuscript was written through contributions of all authors. All authors have given approval to the final version of the manuscript.

Notes

The authors declare no competing financial interest.

ACKNOWLEDGMENTS

The authors acknowledge the funding and technical support from BP through the BP International Centre for Advanced Materials (BP-ICAM), which made this research possible. A portion of this research was carried out in part in the Frederick Seitz Materials Research Laboratory Central Research Facilities, University of Illinois. The authors acknowledge Imaging Technology Group in Beckman Institute for Advanced Science and Technology. The authors acknowledge Dr. Ke Yang, Dr. Xiaocun Lu, Michael T. Odarczenko, and Justin Shang for helpful discussions.

REFERENCES

- (1) White, S. R.; Sottos, N. R.; Geubelle, P. H.; Moore, J. S.; Kessler, M. R.; Sriram, S. R.; Brown, E. N.; Viswanathan, S. Autonomic Healing of Polymer Composites. *Nature* **2001**, *409*, 794–797.
- (2) Jackson, A. C.; Bartelt, J. A.; Braun, P. V. Transparent Self-Healing Polymers Based on Encapsulated Plasticizers in a Thermoplastic Matrix. *Adv. Funct. Mater.* **2011**, *21*, 4705–4711.

- (3) Blaiszik, B. J.; Kramer, S. L. B.; Grady, M. E.; McLroy, D. A.; Moore, J. S.; Sottos, N. R.; White, S. R. Autonomic Restoration of Electrical Conductivity. *Adv. Mater. (Weinheim, Ger.)* **2012**, *24*, 398–401.
- (4) Odom, S. A.; Tyler, T. P.; Caruso, M. M.; Ritchey, J. A.; Schulmerich, M. V.; Robinson, S. J.; Bhargava, R.; Sottos, N. R.; White, S. R.; Hersam, M. C.; Moore, J. S. Autonomic Restoration of Electrical Conductivity Using Polymer-Stabilized Carbon Nanotube and Graphene Microcapsules. *Appl. Phys. Lett.* **2012**, *101*, 043106.
- (5) Yuan, Y. C.; Rong, M. Z.; Zhang, M. Q.; Chen, J.; Yang, G. C.; Li, X. M. Self-Healing Polymeric Materials Using Epoxy/Mercaptan as the Healtant. *Macromolecules* **2008**, *41*, 5197–5202.
- (6) Huang, M.; Yang, J. Facile Microencapsulation of HDI for Self-Healing Anticorrosion Coatings. *J. Mater. Chem.* **2011**, *21*, 11123–11130.
- (7) Zhao, Y.; Fickert, J.; Landfester, K.; Crespy, D. Encapsulation of Self-Healing Agents in Polymer Nanocapsules. *Small* **2012**, *8*, 2954–2958.
- (8) Esser-Kahn, A. P.; Odom, S. A.; Sottos, N. R.; White, S. R.; Moore, J. S. Triggered Release from Polymer Capsules. *Macromolecules* **2011**, *44*, 5539–5553.
- (9) Johnston, A. P.; Such, G. K.; Caruso, F. Triggering Release of Encapsulated Cargo. *Angew. Chem., Int. Ed.* **2010**, *49*, 2664–2666.
- (10) Wang, H. C.; Zhang, Y.; Possanza, C. M.; Zimmerman, S. C.; Cheng, J.; Moore, J. S.; Harris, K.; Katz, J. S. Trigger Chemistries for Better Industrial Formulations. *ACS Appl. Mater. Interfaces* **2015**, *7*, 6369–6382.
- (11) Lv, L. P.; Zhao, Y.; Vilbrandt, N.; Gallei, M.; Vimalanandan, A.; Rohwerder, M.; Landfester, K.; Crespy, D. Redox Responsive Release of Hydrophobic Self-Healing Agents from Polyaniline Capsules. *J. Am. Chem. Soc.* **2013**, *135*, 14198–14205.
- (12) Li, G. L.; Schenderlein, M.; Men, Y.; Möhwald, H.; Shchukin, D. G. Monodisperse Polymeric Core-Shell Nanocontainers for Organic Self-Healing Anticorrosion Coatings. *Adv. Mater. Interfaces* **2014**, *1*, 1300019.
- (13) Snihirova, D.; Lamaka, S. V.; Cardoso, M. M.; Condeço, J. A. D.; Ferreira, H. E. C. S.; De Fatima Montemor, M. PH-Sensitive Polymeric Particles with Increased Inhibitor-Loading Capacity as Smart Additives for Corrosion Protective Coatings for AA2024. *Electrochim. Acta* **2014**, *145*, 123–131.
- (14) Baginska, M.; Blaiszik, B. J.; Odom, S. A.; Esser-Kahn, A. E.; Caruso, M. M.; Moore, J. S.; Sottos, N. R.; White, S. R. Thermoresponsive Microcapsules for Autonomic Lithium-Ion Battery Shutdown. In *Experimental Mechanics on Emerging Energy Systems and Materials, Vol. 5: Proceedings of the 2010 Annual Conference on Experimental and Applied Mechanics*; Proulx, T., Ed.; Springer: New York, 2011; pp 17–23.
- (15) Sagi, A.; Weinstain, R.; Karton, N.; Shabat, D. Self-Immolative Polymers. *J. Am. Chem. Soc.* **2008**, *130*, 5434.
- (16) Weinstain, R.; Sagi, A.; Karton, N.; Shabat, D. Self-Immolative Comb-Polymers: Multiple-Release of Side-Reporters by a Single Stimulus Event. *Chem. - Eur. J.* **2008**, *14*, 6857–6861.
- (17) Dewit, M. A.; Gillies, E. R. A Cascade Biodegradable Polymer Based on Alternating Cyclization and Elimination Reactions. *J. Am. Chem. Soc.* **2009**, *131*, 18327–18334.
- (18) Dewit, M. A.; Beaton, A.; Gillies, E. R. A Reduction Sensitive Cascade Biodegradable Linear Polymer. *J. Polym. Sci., Part A: Polym. Chem.* **2010**, *48*, 3977–3985.
- (19) DiLauro, A. M.; Robbins, J. S.; Phillips, S. T. Reproducible and Scalable Synthesis of End-Cap-Functionalized Depolymerizable Poly-(phthalaldehydes). *Macromolecules* **2013**, *46*, 2963–2968.
- (20) Kaitz, J. A.; Diesendruck, C. E.; Moore, J. S. End Group Characterization of Poly(phthalaldehyde): Surprising Discovery of a Reversible, Cationic Macrocyclization Mechanism. *J. Am. Chem. Soc.* **2013**, *135*, 12755–12761.
- (21) Fan, B.; Trant, J. F.; Wong, A. D.; Gillies, E. R. Polyglyoxylates: A Versatile Class of Triggerable Self-Immolative Polymers from Readily Accessible Monomers. *J. Am. Chem. Soc.* **2014**, *136*, 10116–10123.
- (22) Lee, O. P.; Lopez Hernandez, H.; Moore, J. S. Tunable Thermal Degradation of Poly(vinyl Butyl Carbonate Sulfone)s via Side-Chain Branching. *ACS Macro Lett.* **2015**, *4*, 665–668.
- (23) Lobe, J. M.; Swager, T. M. Radiation Detection: Resistivity Responses in Functional Poly(olefin Sulfone)/carbon Nanotube Composites. *Angew. Chem., Int. Ed.* **2010**, *49*, 95–98.
- (24) Lobe, J. M.; Swager, T. M. Disassembly of Elastomers: Poly(olefin sulfone)–Silicones with Switchable Mechanical Properties. *Macromolecules* **2010**, *43*, 10422–10426.
- (25) Possanza Casey, C. M.; Moore, J. S. Base-Triggered Degradation of Poly(vinyl Ester Sulfone)s with Tunable Sensitivity. *ACS Macro Lett.* **2016**, *5*, 1257–1260.
- (26) DiLauro, A. M.; Abbaspourrad, A.; Weitz, D. A.; Phillips, S. T. Stimuli-Responsive Core-Shell Microcapsules with Tunable Rates of Release by Using a Depolymerizable Poly(phthalaldehyde) Membrane. *Macromolecules* **2013**, *46*, 3309–3313.
- (27) Grolman, J. M.; Inci, B.; Moore, J. S. pH-Dependent Switchable Permeability from Core–Shell Microcapsules. *ACS Macro Lett.* **2015**, *4*, 441–445.
- (28) Dowding, P. J.; Atkin, R.; Vincent, B.; Bouillot, P. Oil Core-Polymer Shell Microcapsules Prepared by Internal Phase Separation from Emulsion Droplets. I. Characterization and Release Rates for Microcapsules with Polystyrene Shells. *Langmuir* **2004**, *20*, 11374–11379.
- (29) Andersson Trojer, M.; Nordstierna, L.; Bergek, J.; Blanck, H.; Holmberg, K.; Nydén, M. Use of Microcapsules as Controlled Release Devices for Coatings. *Adv. Colloid Interface Sci.* **2015**, *222*, 18–43.
- (30) Yow, H. N.; Routh, A. F. Formation of Liquid Core-Polymer Shell Microcapsules. *Soft Matter* **2006**, *2*, 940–949.
- (31) Tasker, A. L.; Hitchcock, J. P.; He, L.; Baxter, E. A.; Biggs, S.; Cayre, O. J. The Effect of Surfactant Chain Length on the Morphology of Poly(methyl Methacrylate) Microcapsules for Fragrance Oil Encapsulation. *J. Colloid Interface Sci.* **2016**, *484*, 10–16.
- (32) Yin, W.; Yates, M. Z. Encapsulation and Sustained Release from Biodegradable Microcapsules Made by Emulsification/freeze Drying and Spray/freeze Drying. *J. Colloid Interface Sci.* **2009**, *336*, 155–161.
- (33) Persico, P.; Carfagna, C.; Danicher, L.; Frere, Y. Polyamide Microcapsules Containing Jojoba Oil Prepared by Inter-Facial Polymerization. *J. Microencapsulation* **2005**, *22*, 471–486.
- (34) Loxley, A.; Vincent, B. Preparation of Poly(methylmethacrylate) Microcapsules with Liquid Cores. *J. Colloid Interface Sci.* **1998**, *208*, 49–62.
- (35) Pekarek, K. J.; Jacob, J. S.; Mathiowitz, E. Double-Walled Polymer Microspheres for Controlled Drug Release. *Nature* **1994**, *367*, 258–260.
- (36) Berkland, C.; Pollauf, E.; Pack, D. W.; Kim, K. Uniform Double-Walled Polymer Microspheres of Controllable Shell Thickness. *J. Controlled Release* **2004**, *96*, 101–111.
- (37) Andersson Trojer, M.; Nordstierna, L.; Nordin, M.; Nydén, M.; Holmberg, K. Encapsulation of Actives for Sustained Release. *Phys. Chem. Chem. Phys.* **2013**, *15*, 17727.
- (38) Li, M.; Rouaud, O.; Poncelet, D. Microencapsulation by Solvent Evaporation: State of the Art for Process Engineering Approaches. *Int. J. Pharm.* **2008**, *363*, 26–39.
- (39) Torza, S.; Mason, S. G. Three Phase Interaction in Shear and Electrical Field. *J. Colloid Interface Sci.* **1970**, *33*, 67–83.
- (40) Chetouani, A.; Hammouti, B.; Benkaddour, M. Corrosion Inhibition of Iron in Hydrochloric Acid Solution by Jojoba Oil. *Pigm. Resin Technol.* **2004**, *33*, 26–31.
- (41) Fundueanu, G.; Constantin, M.; Esposito, E.; Cortesi, R.; Nastuzzi, C.; Menegatti, E. Cellulose Acetate Butyrate Microcapsules Containing Dextran Ion-Exchange Resins as Self-Propelled Drug Release System. *Biomaterials* **2005**, *26*, 4337–4347.
- (42) Chu, L.; Utada, A. S.; Shah, R. K.; Kim, J.; Weitz, D. A. Controllable Monodisperse Multiple Emulsions. *Angew. Chem.* **2007**, *119*, 9128–9132.
- (43) Shah, R. K.; Kim, J.; Agresti, J. J.; Weitz, D. A.; Chu, L. Fabrication of Monodisperse Thermosensitive Microgels and Gel Capsules in Microfluidic Devices. *Soft Matter* **2008**, *4*, 2303–2309.

(44) Lopez Hernandez, H.; Kang, S. K.; Lee, O. P.; Hwang, S. W.; Kaitz, J. A.; Inci, B.; Park, C. W.; Chung, S.; Sottos, N. R.; Moore, J. S.; et al. Triggered Transience of Metastable Poly(phthalaldehyde) for Transient Electronics. *Adv. Mater. (Weinheim, Ger.)* **2014**, *26*, 7637–7642.

(45) Park, C. W.; Kang, S. K.; Hernandez, H. L.; Kaitz, J. A.; Wie, D. S.; Shin, J.; Lee, O. P.; Sottos, N. R.; Moore, J. S.; Rogers, J. A.; et al. Thermally Triggered Degradation of Transient Electronic Devices. *Adv. Mater. (Weinheim, Ger.)* **2015**, *27*, 3783.

(46) Seefeldt, S. S.; Jensen, J. E.; Fuerst, E. P. Log-Logistic Analysis of Herbicide Dose-Response Relationships. *Weed Technol.* **1995**, *9*, 218–227.